Title

Isolation of muscle stem cells from rat skeletal muscles

Authors

Sesillo, Francesca Boscolo
Wong, Michelle
Cortez, Amy
et al.

Publication Date

2020-03-01

DOI

10.1016/j.scr.2019.101684

Peer reviewed

HHS Public Access

Author manuscript

Stem Cell Res. Author manuscript; available in PMC 2020 July 13.

Published in final edited form as:

Stem Cell Res. 2020 March ; 43: 101684. doi:10.1016/j.scr.2019.101684.

Isolation of muscle stem cells from rat skeletal muscles

Francesca Boscolo Sesillo[a], **Michelle Wong**[a], **Amy Cortez**[b], **Marianna Alperin**[a,*]

[a]Department of Obstetrics, Gynecology, and Reproductive Sciences, Division of Female Pelvic Medicine and Reconstructive Surgery, University of California San Diego, La Jolla, CA 92093, USA

[b]Flow Cytometry Core, Sanford Burnham Prebys Medical Discovery Institute, La Jolla, CA 92037, USA

Abstract

Muscle stem cells (MuSCs) are involved in homeostatic maintenance of skeletal muscle and play a central role in muscle regeneration in response to injury. Thus, understanding MuSC autonomous properties is of fundamental importance for studies of muscle degenerative diseases and muscle plasticity. Rat, as an animal model, has been widely used in the skeletal muscle field, however rat MuSC isolation through fluorescence-activated cell sorting has never been described. This work validates a protocol for effective MuSC isolation from rat skeletal muscles. Tibialis anterior was harvested from female rats and digested for isolation of MuSCs. Three protocols, employing different cell surface markers (CD106, CD56, and CD29), were compared for their ability to isolate a highly enriched MuSC population. Cells isolated using only CD106 as a positive marker showed high expression of Pax7, ability to progress through myogenic lineage while in culture, and complete differentiation in serum-deprived conditions. The protocol was further validated in gastrocnemius, diaphragm, and the individual components of the pelvic floor muscle complex (coccygeus, iliocaudalis, and pubocaudalis), proving to be reproducible. CD106 is an efficient marker for reliable isolation of MuSCs from a variety of rat skeletal muscles.

*Corresponding author. malperin@ucsd.edu (M. Alperin).

CRediT authorship contribution statement

Francesca Boscolo Sesillo: Conceptualization, Data curation, Formal analysis, Resources, Writing - original draft, Writing - review & editing. **Michelle Wong:** Resources, Writing - review & editing. **Amy Cortez:** Resources, Writing - review & editing. **Marianna Alperin:** Conceptualization, Data curation, Formal analysis, Writing - review & editing.

Declarations

Ethical approval and consent to participate: All animal protocols were approved by The University of California San Diego Institutional Animal Care and Use Committee.

Consent for publication

Not applicable.

Data for reference

The data used and analyzed in the current study are available upon request.

Declaration of Competing Interest

The authors declare that they have no competing interests.

Supplementary materials

Supplementary material associated with this article can be found, in the online version, at doi:10.1016/j.scr.2019.101684.

Keywords

Muscle stem cells; Flow cytometry; Rat; CD106; Pelvic floor muscles

1. Introduction

Muscle stem cells (MuSCs), which reside between the sarcolemma and basal lamina, are required for the maintenance of adult muscle and muscle regeneration after injury (Mauro, 1961; Cheung and Rando, 2013). MuSCs exist in a tightly regulated quiescent state (Cheung and Rando, 2013). MuSC activation and proliferation is induced in response to increased mechanical load or to muscle injury (Relaix and Zammit, 2012; Tatsumi et al., 2001). Upon activation, MuSCs progress through the myogenic lineage until fusion with damaged myofibers occurs and muscle repair is achieved (Relaix and Zammit, 2012). The activation and differentiation of MuSCs has been extensively studied leading to the identification of sequentially expressed markers specific to each step of this process. Pax7, a transcription factor expressed by quiescent and early-activated MuSCs, is required for their functionality in homeostatic and regenerating conditions. Indeed, lack of Pax7 expression in MuSCs *in vivo* results in the absence of muscle regeneration following injury (Lepper et al., 2011; Seale et al., 2000). Upon activation, expression of MyoD, a transcription factor responsible for early commitment, promotes MuSC entry into the cell cycle (Cornelison and Wold, 1997). Finally, myogenin is activated, inducing terminal differentiation of MuSCs that can fuse together to form new myofibers or fuse with the existing myofibers.

Studies of MuSCs autonomous properties rely mainly on the use of fluorescence-activated cell sorting (FACS). Isolation of MuSCs has been described in mouse, human, pig, and cow (Liu et al., 2015; Alexander et al., 2016; Uezumi et al., 2016; Ding et al., 2017; Ding et al., 2018; Maesner et al., 2016). A wide array of cell surface proteins have been reported as positive markers for MuSC identification and isolation, namely β1-integrin (CD29), CXCR4 (CD184), VCAM-1 (CD106), NCAM (CD56), α-7 integrin, CD34, tetraspanin (CD82), and CD318. Negative selection markers are conserved among laboratories and different mammalian species and include CD45 (lymphocytes), CD31 (endothelial cells), CD11b (macrophages), and Sca1 (fibro-adi-pogenic progenitors). Despite the extensive knowledge of MuSC identification markers and the broad spectrum of protocols employed for their isolation among multiple species, purification of MuSCs from rat has never been reported.

The rat model has been extensively used in skeletal muscle research (Homberg et al., 2017). Rat, compared to other rodents, better recapitulates human muscle in architecture, physiology, and anatomy, making it a better model to study skeletal muscles. Muscle architecture (macroscopic arrangement of muscle fibers), which is fundamental for *in vivo* muscle function, has been shown to be similar between rats and humans, when compared to other animal models (Lieber and Friden, 2000). Comparative studies of abdominal muscles revealed a high degree of similarity within the same muscle groups between rat and human. The major architectural parameters (physiological cross sectional area, operational sarcomere length, and fiber orientation) were comparable, despite differences in body size and muscle mass (Brown et al., 2010). Additionally, studies of the female pelvic floor

muscles showed that rats, compared to other commonly used laboratory animals, such as rabbit and mouse, were the closest to humans in terms of muscle design (Alperin et al., 2014). Moreover, the architectural difference index of rat pelvic floor muscles, which quantifies how closely rat muscle architecture resembles human muscle architecture, was comparable to that of non-human primates (Brown et al., 2010; Stewart et al., 2017). Furthermore, rat and human *in vivo* response to exercise shows similar qualitative and quantitative changes in plasma volume and blood biochemical parameters (Goutianos et al., 2015). Additionally, the rat physiology is closer to human physiology than mouse is, making rat a widely employed preclinical model for toxicology and safety studies (Noto et al., 2018). Indeed, like in human, the rat genome contains genes involved in protein breakdown and detection and detoxification of chemicals that have been lost in the mouse genome (Gibbs et al., 2004). Finally, rats are 10-fold larger than mice, which facilitates a wider variety of experimental procedures, collection of larger samples, and study of rare cell populations or low abundance molecules. The larger size of the rat also enables multiple concomitant measurements in a single animal, thus, reducing the number of animals needed.

Given that the rat model is widely used in studies focused on skeletal muscles (Dwinell et al., 2011), we aimed to develop and validate an efficient and reliable protocol for MuSC isolation from the rat. The central role of MuSCs in the maintenance of muscle homeostasis and regeneration makes isolation and study of MuSC autonomous properties of fundamental importance. Here, we describe for the first time a method for isolation of rat MuSCs via FACS that relies on a single positive marker (VCAM-1 (CD106)) for identification of this cell population.

2. Materials and methods

2.1. Animals

Female 3-months old Sprague-Dawley rats (Envigo) were euthanized via CO2 inhalation followed by thoracotomy. Hind limb muscles (tibialis anterior (TA), gastrocnemius (GAS) and quadriceps), diaphragm (DIA), and pelvic floor muscles (coccygeus (C), iliocaudalis (ICa), and pubocaudalis (PCa)) were harvested. The University of California San Diego Institutional Animal Care and Use Committee approved all study procedures.

2.2. Cell isolation

Muscle stem cells (MuSCs) were isolated as described in Gromova et al., 2015 with minor modifications (Gromova et al., 2015). Cell isolation was performed using Ham's F-10 supplemented with 10% horse serum. TA, GAS, DIA, C, ICa, and PCa were individually minced and incubated in 700 units/ml collagenase type II solution for 1.5 h and collagenase and dispase II solution (100 units/mL and 2 units/mL, respectively) for 30 min. Tissue was then passed through a 20 G needle and a 70 μm nylon filter. Antibody incubation was performed in 1 mL volume for 1 h.

The positive markers used to identify the MuSCs were CD29, CD56, and CD106. The negative selection markers used to identify hematopoietic and endothelial cells were CD45, CD11b, and CD31. Antibody titration was performed with LSR Fortessa (BD Biosciences,

USA). Multiple antibody concentrations were tested: 0.5, 1, 1.5, 2, 3 μg per 10^6 cells for the individual positive and negative markers; and 0.1, 0.2, 0.3, 0.4, 0.5 μg per 10^6 cells for the negative markers in combination. Proper antibody concentration was chosen using the stain index (*FI*: fluorescent intensity):

$$n\ index = \frac{(FI\ positive\ population - FI\ negative\ population)}{2\ x\ standarad\ deviation\ negative\ population}$$

MuSCs were isolated with FACSAria II (BD Biosciences, USA) cell sorter employing three different protocols. Protocol 1: Lin^- / $CD106^+$; Protocol 2: Lin^- / $CD56^+$ / $CD29^+$; and Protocol 3: Lin^- / $CD106^+$ / $CD29^+$ (Lin^-: $CD45^-$ / $CD11b^-$ / $CD31^-$). We performed 3 separate isolations for each muscle analyzed.

2.3. Cell culture

Cells were plated (2500 cells/well) in laminin coated 96-well plates in growth media (40% DMEM (Dulbecco's modified Eagle's medium), 40% Ham's F-10, 20% fetal bovine serum, 1% Pen/Strep (penicillin/streptomycin), 25 ng/mL basic fibroblast growth factor.) Cells were fixed 2, 12, 72, and 120 h after isolation to determine expression of myogenic markers. Myogenic differentiation was induced on 10000 cells 12 h after isolation, employing differentiation media (DMEM, 2% horse serum, 1% Pen/Strep) as previously described (Boscolo Sesillo et al., 2019), and assessed 72 h later.

2.4. Immunostaining

Frozen tissue sections were fixed with 4% paraformaldehyde (PFA), washed in PBS (phosphate-buffered saline), and incubated for 1 h with blocking buffer (20% goat serum + 0.3% Triton X-100 in PBS) before overnight incubation with laminin primary antibody (1:200) in blocking buffer. After 3 PBS washes, the slides were incubated for 2 h with secondary antibody (Alexa Fluor 546 goat anti-rabbit IgG) in blocking buffer. After another PBS wash, the slides were post-fixed with 4% PFA, washed again and immersed in boiling antigen unmasking solution for 15 min. Slides were then washed in PBS and incubated with blocking buffer (1 h), followed by Pax7 antibody (1:100) overnight. After 3 PBS washes, the slides were incubated for 2 h with secondary antibody (Alexa Fluor 488 goat anti-mouse IgG) in blocking buffer. Cultured cells were fixed with 4% PFA, washed in PBS, and incubated with blocking buffer (1 h), followed by Pax7 (1:100), MyoD (1:100), Myogenin (1:100), or MyHC (1:100) overnight. Secondary antibodies (Alexa 546 goat anti-mouse IgG and Alexa 488 goat anti-mouse IgG) were incubated at 1:250 dilutions in blocking buffer. Nuclei were identified with DAPI (1:1000).

2.5. RNA isolation and analysis

RNA isolation was performed on freshly isolated cells with miRNeasy Micro kit per manufacturer protocol. QIAxpert was employed for RNA quantification. cDNA was obtained with SuperScript VILO cDNA Synthesis kit, and SYBR green PCR master Mix was used for qRT-PCR.

2.6. Imaging

Imaging was carried out using the Keyence BZX710 microscope (Keyence, Japan). Quantification was performed on 5–8 unmodified images per well (10X magnification) with Adobe Photoshop CS4 and ImageJ.

2.7. Statistical analysis

Data were compared between groups using one- or two-way ANOVA, followed by pairwise comparisons with Tukey's range test when appropriate, with significance set to 5%. All statistical analyses were performed with Prism 8.

Key resources table containing vendor and catalog number for all commercial products used in this study is provided.

3. Results

We first assessed *in situ* localization of MuSCs in the rat tibialis anterior (TA). Visual assessment of ~300 MuSCs indicated that all $Pax7^+$ cells localized under the basal lamina with none present in the interstitial space, similar to mouse MuSCs (Fig. 1) (Yin et al., 2013). Quantification of MuSCs in rat TA revealed an average of 10 $Pax7^+$ cells per mm^2. Our results are comparable to mouse, where the density of MuSCs ranges from 5 to 20 cells/mm^2 (Fig. 1) (Parisi et al., 2015; Eliazer et al., 2019; Schaaf et al., 2018).

3.1. Determination of reliable positive markers for rat MuSC isolation

To isolate a highly enriched MuSC population, we identified commercially available antibodies suitable in rat and tested them on pooled preparations of TA, GAS, and quadriceps to determine antibody binding specificity and optimal concentrations (Figure S1). First, CD106, CD56, and CD29 antibodies were titrated through flow cytometry to confirm the expression of each marker in the muscles. Analyses were performed on the LSR Fortessa where non-treated controls were compared to cells treated with one of the five progressively increasing antibody concentrations (0.5, 1, 1.5, 2, and 3 μg per 10^6 cells) (Figs. S1A–S1C). Based on the stain index, the optimal concentration for all antibodies was 1.5 μg per 10^6 cells. Similarly, we titrated antibodies for the negative selection markers: CD31, CD45, and CD11b. Each antibody was tested separately (Figs. S1D–S1F) to assess binding specificity, and in combination to ensure that simultaneous use of multiple antibodies did not cause signal saturation (Fig. S1G). Optimal staining was achieved with 0.3 μg per 10^6 cells for each antibody.

Guided by protocols from other models, we tested three isolation strategies in the rat TA. Protocol 1 relied on CD106 as the only positive marker. In Protocols 2 and 3, cells were concurrently stained for CD56 and CD29 or CD106 and CD29, respectively (Fig. 2A). We used single color and fluorescence minus one (FMO) controls to determine the gating system (Figure S1K–M). Using forward and side scatter parameters independent of fluorescent signal, we first excluded cellular debris and cell clusters (Fig. 2B–D, three top plots). For Protocol 1, we used DAPI negative staining to identify live cells. Within the live cell population, we then determined which lineage negative cells ($CD31^-$/$CD45^-$/$CD11b^-$,

Lin$^-$) expressed CD106 (Fig. 2B). Employing Protocol 1, we identified a single putative MuSC population (P1). For Protocols 2 and 3, we utilized the lack of negative selection markers and DAPI expression to identify live Lin$^-$ cells, coupled with the expression of both positive markers to discern the presumed MuSC populations. Interestingly, expression of the CD56 marker (Protocol 2) was detectable in samples prepared from pooled hind limb muscle homogenate, but not in samples derived from TA alone, suggesting that CD56 is not conserved among different muscles. We, therefore, excluded CD56 from further experiments. In Protocol 2, we observed a clear separation of two cell populations based on CD29 expression (Fig. 2C). Using Protocol 3, we also identified two cells populations: one positive for both CD29 and CD106 and the other positive only for CD29 (Fig. 2D). We went on to further examine the following subpopulations: CD29^{High} (P2) and CD29^{Low} (P2b) identified using Protocol 2, and CD106$^+$/CD29$^+$ (P3) and CD106$^-$/CD29$^+$ (P3b) identified using Protocol 3 (Fig. 2C and D).

3.2. CD106 is a valid marker for isolation of rat MuSCs from tibialis anterior muscle

To test cell identity and myogenic commitment of the 5 cell populations (P1, P2, P2b, P3, and P3b) described above, we isolated cells from TA using BD Biosciences FACSAria II cell sorter. First, we compared the percentage of putative MuSCs sorted using our three different protocols (Fig. S2A). Protocols 1 and 3 yielded 1.6% for P1 (CD106$^+$) and P3 (CD106$^+$/CD29$^+$) populations, which was significantly lower than 6.5% putative MuSCs isolated employing Protocol 2 (CD29^{High}) (Figure S2A). P2b (CD29^{Low}) constituted 9.3% and P3b (CD106$^-$/CD29$^+$) 12.4% of the original sorted population (Fig. S2A). After isolation, cells were plated and fixed either 2 or 12 h later to assess cell identity or cultured in growth conditions for 3 and 5 days to determine their myogenic potential (Fig. 3A). Expression of Pax7 in freshly isolated P1, P2, and P3 populations was ~90% and 80% 2 and 12 h after isolation, respectively (Fig. 3B). In contrast, only 20% of P2b (CD29^{Low}) and 50% of P3b (CD106$^-$/CD29$^+$) populations expressed Pax7 2 h after isolation (Figure S2B). These results suggest that P1, P2, and P3 populations represent a highly enriched MuSCs population, whereas, only up to a half of the P2b and P3b cells were potential MuSCs. Thus, using CD29^{Low} or CD106$^-$/CD29$^+$ precludes efficient isolation of a highly enriched population.

To assess the ability of the isolated cells to progress through myogenic lineage, cells cultured in growth media for 3 and 5 days were assessed for the expression of MyoD and myogenin, respectively. Around 80% of P1, P2, and P3 populations expressed MyoD, whereas less than 40% of the P2b and P3b cells expressed MyoD (Fig. 3C and S2C). Moreover, 20% of P1, P2, and P3 cells expressed myogenin, while myogenin was detected in less than 1% of P2b and P3b populations (Fig. 3D and S2D). Taken together, these data show that only CD106$^+$ (P1), CD29^{High} (P2), and CD106$^+$/CD29$^+$ (P3) cells express high levels of Pax7 and are capable of efficiently progressing through the myogenic lineage *in vitro*.

To determine the ability of P1, P2, and P3 populations to complete myogenic differentiation, we placed cells in serum-deprived media for 3 days. Myosin heavy chain (MyHC), a marker of terminal differentiation, was used to calculate the differentiation index ((nuclei of MyHC$^+$ cells/total nuclei number)*100) (Fig. 3E). P1 and P3 differentiation index was over 60%,

compared to only 40% in the P2 population (Fig. 3F). Moreover, P2 cells demonstrated a lower ability to fuse, evidenced by sparse appearance of the myotubes relative to the P1 and P3 populations. (Fig. S2F). Consistent with their low ability to undergo myogenic commitment, the differentiation index of P2b and P3b cells was less than 2% (Fig. S2E). These results indicate that Protocols 1 and 3 accurately identify rat MuSCs capable of myogenic commitment and terminal differentiation.

Despite high expression of Pax7, P2 ($CD29^{High}$) cells were not capable of efficient differentiation or fusion compared to P1 and P3 populations. To investigate potential mechanisms underlying these differences, we analyzed myogenic gene expression by qRT-PCR on cells freshly isolated using all three protocols (Fig. 3G). A significant increase in myogenin expression was observed in the P2 population relative to P1 and P3 populations. Moreover, a trend towards reduced Pax7 gene expression was noted in P2 compared to P1 and P3 cells. These results suggest that P2 cells are more committed than P1 and P3 populations. Given that Protocol 2 led to the isolation of less undifferentiated cells that could not undergo efficient myogenic differentiation (Fig. 3F and G), this protocol was excluded from further analyses.

While Protocol 1 relies solely on CD106 as a positive isolation marker, Protocol 3 depends on two positive markers: CD106 and CD29. Importantly, cells obtained from both protocols did not differ phenotypically, indicating that both protocols yield comparable MuSC populations. Given fiscal and technical advantages of employing a single positive marker for the identification of MuSCs, we focused on validating Protocol 1 in five additional rat muscles.

3.3. MuSCs can be efficiently isolated from a broad range of rat skeletal muscles employing CD106 as a single positive marker

To validate our selected protocol, we tested its reliability and efficiency in isolating MuSCs from other rat skeletal muscles, specifically GAS, DIA, and the individual pelvic floor muscles (C, ICa, and PCa). To enhance population separation during isolation, which increases MuSC yield, we first optimized the gating for Protocol 1 (Fig. 4A). Based on MuSC size, determined during the initial experiments (Fig. 2B), we applied a gate to select for live small cells. Further gates were progressively designed to define single cell populations, Lin^{-} cells, and $CD106^{+}$ cells. This new gating system was reproducible among all muscles evaluated, leading to a consistent isolation of 2–3% of MuSC from the initial number of cells and improving upon 1.6% yield from the previous gating system (Fig. 4B, Figure S2A and Figure S3A). Upon isolation, cells were plated in growth media for 2 h, fixed, and assessed for Pax7 expression to evaluate their identity (Fig. 4C). Consistent with the results obtained for TA, ~90% of cells isolated from all other muscles expressed Pax7 (Fig. 4D). Moreover, high expression of MyoD and myogenin was present when the cells were placed in culture for 3 and 5 days, respectively (Figs. S3B–S3E). Cells placed in serum-deprived media for 3 days exhibited a differentiation index between 70 and 80% (Fig. 4E and F). These results confirm that Protocol 1 can be reliably employed in different muscles in the rat model for isolation of a highly enriched MuSC population capable of myogenic commitment and terminal differentiation.

4. Discussion

The positive markers selected for our studies were based on the existing literature and antibody availability for rat, and included vascular cell adhesion molecule (VCAM-1, CD106), neural cell adhesion molecule (NCAM, CD56), and β1-integrin (CD29). CD106 is a trans-membrane protein in the immunoglobulin superfamily that has been successfully used for isolation of mouse MuSCs (Liu et al., 2015). Importantly, expression of this protein in quiescent cells is required for maintenance of their basal function and prevention of premature lineage progression (Choo et al., 2017). The current study demonstrates, for the first time, that CD106 is a reliable marker for the isolation of a highly enriched MuSC population from various rat skeletal muscles. Indeed, $CD106^{+}/CD45^{-}/CD31^{-}/CD11b^{-}$ cells express Pax7 at high levels and are capable of myogenic commitment and full differentiation into myotubes.

CD56 has been mainly described as a marker of quiescent human MuSCs (Alexander et al., 2016; Uezumi et al., 2016). In rodents, expression of this marker has been associated only with MuSCs activated in response to either differentiation stimuli *in vitro* or denervation *in vivo* (Capkovic et al., 2008; Covault and Sanes, 1985). While we observed CD56 expression when analyzing whole muscle cell preparations (Fig. S1C), expression was not found in Lin^{-} gated cells during the sorting process. CD56 is likely expressed in the neuromuscular junctions and not in the MuSCs that we want to isolate (Covault and Sanes, 1985). CD29, has been previously used for the isolation of MuSCs from mouse, pig, and cow (Ding et al., 2017, 2018; Maesner et al., 2016). It is a member of the integrin family and interacts with collagen, fibronectin, and laminin depending on its heterodimer binding partner (Hynes, 2002). It is highly expressed in MuSCs and is necessary for maintenance of quiescence in homeostatic conditions and cell proliferation after injury (Rozo et al., 2016). Moreover, in myoblasts, CD29 is indispensable for cell fusion (Schwander et al., 2003). In contrast to the previous studies, we found that $CD29^{High}$ cells have reduced Pax7 and increased myogenin gene expression (Fig. 3G), and fuse less. The antibody used for the isolation of cells in Protocol 2 is specific for $\alpha_4\beta_1$ integrin immunogen, preferentially selecting for cells expressing the α_4 subunit in association with CD29. The resultant cell population is therefore enriched for $\alpha_4\beta_1$ integrin, while being depleted off α_5-$\alpha_7\beta_1$ integrins. Previous work suggests that the interplay between integrin heterodimers is essential for proper myogenic differentiation and fusion (Yang et al., 1996). We believe that the lack of integrin heterodimer heterogeneity in P2 cells accounts for the phenotype observed in our experiments.

Currently, the majority of MuSC studies are performed in a mouse, owing to the opportunities for genetic manipulation of this model (Huang et al., 2011). However, the small size of these animals significantly limits the amount of muscle tissue, which in turn restricts the number of MuSCs that can be isolated making it hard to perform experiments demanding large cell numbers, such as RNA or ChIP sequencing. The insufficient yield of MuSCs from small mouse muscles necessitates pooling of different muscles from the same animal or pooling of the same muscle type from multiple animals (van Velthoven et al., 2017; Sampath et al., 2018). Pooling different specimens masks the intrinsic variability of different muscles or individual organisms, potentially affecting results and their

interpretation. Moreover, given recent evidence that MuSCs are highly heterogeneous, maintaining muscle and animal identity in future studies could enhance our understanding of diverse MuSC populations (Cornelison and Wold, 1997; Kuang et al., 2007). Using the rat model (10 times larger than a mouse) can help scientists circumvent these limitations and expand the existing studies to smaller muscles previously set aside due to technical constraints. For instance, the regenerative potential of MuSCs from extensor digitorum longus and soleus, small muscles that differ with respect to MuSC number and fiber phenotype, have never been directly compared (Yin et al., 2013, Soukup et al., 2002).

Using our optimized protocol, we obtain a proportion of the sorted cells similar to the mouse (Fig. 4A and S3A) (Liu et al., 2015). Our *in situ* evaluations (Fig. 1) showed an average of 10 $Pax7^+$ cells per mm^2, which is also comparable to the number of MuSCs per mm^2 in mouse (Parisi et al., 2015; Eliazer et al., 2019; Schaaf et al., 2018). Given the above and the larger size of the rat muscles, one can isolate a greater number of MuSCs from the rat. This opens new avenues for investigations focused on the autonomous function of MuSCs derived from small-sized muscles. Larger animal models, such as non-human primates, pig, or cow, would, of course, allow isolation of an even greater number of MuSCs. However, these models are costly relative to the rat, and numerous constraints related to housing and handling of these species exist.

5. Conclusions

In conclusion, a single positive selection marker can be used to reliably isolate MuSCs from a variety of rat skeletal muscles. The use of the rat model for the study of MuSCs offers a major advantage to the skeletal muscle research field, enabling investigations of single muscles of different sizes and individual animals.

Supplementary Material

Refer to Web version on PubMed Central for supplementary material.

Acknowledgments

We thank Ms. Varsha Rajesh for creating and providing the rat image used in this manuscript and the images used for the graphical abstract. University of California San Diego Microscopy shared resources is supported by the NCI Cancer Center Support Grant P30 2P30CA023100-28 to UCSD Moores Cancer Center.

Funding

The authors gratefully acknowledge funding by the National Institute of Health/ Eunice Kennedy Shriver National Institute of Child Health and Human Development, grants R01HD092515 and R21HD094566, for the conduct of this research.

Glossary

MuSC	muscle stem cell
FACS	fluorescent activated cell sorting
FMO	fluorescence minus one

TA	tibialis anterior
GAS	gastrocnemious
DIA	diaphragm
C	coccygeus
ICa	iliocaudalis
PCa	pubocaudalis
P1	Population from protocol 1 (CD106+)
P2	Population from protocol 2 ($CD29^{High}$)
P2b	Population from protocol 2 ($CD29^{Low}$)
P3	Population from protocol 3 (CD106+/CD29+)
P3b	Population from protocol 3 (CD106−/CD29+)

References

Mauro A, 1961 Satellite cell of skeletal muscle fibers. J. Biophys. Biochem. Cytol 9, 493–495. [PubMed: 13768451]

Cheung TH, Rando TA, 2013 Molecular regulation of stem cell quiescence. Nat. Rev. Mol. Cell Biol 14 (6), 329–340. [PubMed: 23698583]

Relaix F, Zammit PS., 2012 Satellite cells are essential for skeletal muscle regeneration: the cell on the edge returns centre stage. Development 139 (16), 2845–2856. [PubMed: 22833472]

Tatsumi R, Sheehan SM, Iwasaki H, Hattori A, Allen RE, 2001 Mechanical stretch induces activation of skeletal muscle satellite cells in vitro. Exp. Cell Res 267 (1), 107–114. [PubMed: 11412043]

Lepper C, Partridge TA, Fan CM, 2011 An absolute requirement for Pax7-positive satellite cells in acute injury-induced skeletal muscle regeneration. Development 138 (17), 3639–3646. [PubMed: 21828092]

Seale P, Sabourin LA, Girgis-Gabardo A, Mansouri A, Gruss P, Rudnicki MA, 2000 Pax7 is required for the specification of myogenic satellite cells. Cell 102 (6), 777–786. [PubMed: 11030621]

Cornelison DD, Wold BJ, 1997 Single-cell analysis of regulatory gene expression in quiescent and activated mouse skeletal muscle satellite cells. Dev. Biol 191 (2), 270–283. [PubMed: 9398440]

Liu L, Cheung TH, Charville GW, Rando TA, 2015 Isolation of skeletal muscle stem cells by fluorescence-activated cell sorting. Nat. Protoc 10 (10), 1612–1624. [PubMed: 26401916]

Alexander MS, Rozkalne A, Colletta A, Spinazzola JM, Johnson S, Rahimov F, et al., 2016 CD82 is a marker for prospective isolation of human muscle satellite cells and is linked to muscular dystrophies. Cell Stem Cell 19 (6), 800–807. [PubMed: 27641304]

Uezumi A, Nakatani M, Ikemoto-Uezumi M, Yamamoto N, Morita M, Yamaguchi A, et al., 2016 Cell-surface protein profiling identifies distinctive markers of progenitor cells in human skeletal muscle. Stem Cell Rep 7 (2), 263–278.

Ding S, Wang F, Liu Y, Li S, Zhou G, Hu P, 2017 Characterization and isolation of highly purified porcine satellite cells. Cell Death Discov 3, 17003. [PubMed: 28417015]

Ding S, Swennen GNM, Messmer T, Gagliardi M, Molin DGM, Li C, et al., 2018 Maintaining bovine satellite cells stemness through p38 pathway. Sci. Rep 8 (1), 10808. [PubMed: 30018348]

Maesner CC, Almada AE, Wagers AJ, 2016 Established cell surface markers efficiently isolate highly overlapping populations of skeletal muscle satellite cells by fluorescence-activated cell sorting. Skelet. Muscle 6, 35. [PubMed: 27826411]

Homberg JR, Wohr M, Alenina N, 2017 Comeback of the rat in biomedical research. ACS Chem. Neurosci 8 (5), 900–903. [PubMed: 28182397]

Lieber RL, Friden J, 2000 Functional and clinical significance of skeletal muscle architecture. Muscle Nerve 23 (11), 1647–1666. [PubMed: 11054744]

Brown SH, Banuelos K, Ward SR, Lieber RL, 2010 Architectural and morphological assessment of rat abdominal wall muscles: comparison for use as a human model. J. Anat 217 (3), 196–202. [PubMed: 20646108]

Alperin M, Tuttle LJ, Conner BR, Dixon DM, Mathewson MA, Ward SR, et al., 2014 Comparison of pelvic muscle architecture between humans and commonly used laboratory species. Int. Urogynecol. J 25 (11), 1507–1515. [PubMed: 24915840]

Stewart AM, Cook MS, Esparza MC, Slayden OD, Alperin M, 2017 Architectural assessment of rhesus macaque pelvic floor muscles: comparison for use as a human model. Int. Urogynecol. J 28 (10), 1527–1535. [PubMed: 28285397]

Goutianos G, Tzioura A, Kyparos A, Paschalis V, Margaritelis NV, Veskoukis AS, et al., 2015 The rat adequately reflects human responses to exercise in blood biochemical profile: a comparative study. Physiol. Rep 3 (2).

Noto FK, Adjan-Steffey V, Tong M, Ravichandran K, Zhang W, Arey A, et al., 2018 Sprague Dawley Rag2-null rats created from engineered spermatogonial stem cells are immunodeficient and permissive to human xenografts. Mol. Cancer Ther 17 (11), 2481–2489. [PubMed: 30206106]

Gibbs RA, Weinstock GM, Metzker ML, Muzny DM, Sodergren EJ, Scherer S, et al., 2004 Genome sequence of the Brown Norway rat yields insights into mammalian evolution. Nature 428 (6982), 493–521. [PubMed: 15057822]

Dwinell MR, Lazar J, Geurts AM, 2011 The emerging role for rat models in gene discovery. Mamm. Genome 22 (7–8), 466–475. [PubMed: 21732192]

Gromova A, Tierney MT, Sacco A, 2015 FACS-based satellite cell isolation from mouse hind limb muscles. Bio Protoc 5 (16).

Boscolo Sesillo F, Fox D, Sacco A, 2019 Muscle stem cells give rise to rhabdomyosarcomas in a severe mouse model of Duchenne muscular dystrophy. Cell Rep 26 (3), 689–701 e6. [PubMed: 30650360]

Yin H, Price F, Rudnicki MA, 2013 Satellite cells and the muscle stem cell niche. Physiol. Rev 93 (1), 23–67. [PubMed: 23303905]

Parisi A, Lacour F, Giordani L, Colnot S, Maire P, Le Grand F, 2015 APC is required for muscle stem cell proliferation and skeletal muscle tissue repair. J. Cell Biol 210 (5), 717–726. [PubMed: 26304725]

Eliazer S, Muncie JM, Christensen J, Sun X, D'Urso RS, Weaver VM, et al., 2019 Wnt4 from the Niche Controls the mechano-properties and quiescent state of muscle stem cells. Cell Stem Cell

Schaaf GJ, van Gestel TJM, In 't Groen SLM, de Jong B, Boomaars B, Tarallo A, et al., 2018 Satellite cells maintain regenerative capacity but fail to repair disease-associated muscle damage in mice with Pompe disease. Acta Neuropathol. Commun 6 (1), 119. [PubMed: 30404653]

Choo HJ, Canner JP, Vest KE, Thompson Z, Pavlath GK, 2017 A tale of two niches: differential functions for VCAM-1 in satellite cells under basal and injured conditions. Am. J. Physiol. Cell Physiol 313 (4), C392–C404. [PubMed: 28701357]

Capkovic KL, Stevenson S, Johnson MC, Thelen JJ, Cornelison DD, 2008 Neural cell adhesion molecule (NCAM) marks adult myogenic cells committed to differentiation. Exp. Cell Res 314 (7), 1553–1565. [PubMed: 18308302]

Covault J, Sanes JR, 1985 Neural cell adhesion molecule (N-CAM) accumulates in denervated and paralyzed skeletal muscles. Proc. Natl. Acad. Sci. USA 82 (13), 4544–4548. [PubMed: 3892537]

Hynes RO, 2002 Integrins: bidirectional, allosteric signaling machines. Cell 110 (6), 673–687. [PubMed: 12297042]

Rozo M, Li L, Fan CM, 2016 Targeting beta1-integrin signaling enhances regeneration in aged and dystrophic muscle in mice. Nat. Med 22 (8), 889–896. [PubMed: 27376575]

Schwander M, Leu M, Stumm M, Dorchies OM, Ruegg UT, Schittny J, et al., 2003 Beta1 integrins regulate myoblast fusion and sarcomere assembly. Dev. Cell 4 (5), 673–685. [PubMed: 12737803]

Yang JT, Rando TA, Mohler WA, Rayburn H, Blau HM, Hynes RO, 1996 Genetic analysis of alpha 4 integrin functions in the development of mouse skeletal muscle. J. Cell Biol 135 (3), 829–835. [PubMed: 8909554]

Huang G, Tong C, Kumbhani DS, Ashton C, Yan H, Ying QL, 2011 Beyond knockout rats: new insights into finer genome manipulation in rats. Cell Cycle 10 (7), 1059–1066. [PubMed: 21383544]

van Velthoven CTJ, de Morree A, Egner IM, Brett JO, Rando TA, 2017 Transcriptional Profiling of Quiescent Muscle Stem Cells In Vivo. Cell Rep 21 (7), 1994–2004. [PubMed: 29141228]

Sampath SC, Sampath SC, Ho ATV, Corbel SY, Millstone JD, Lamb J, et al., 2018 Induction of muscle stem cell quiescence by the secreted niche factor Oncostatin M. Nat. Commun 9 (1), 1531. [PubMed: 29670077]

Kuang S, Kuroda K, Le Grand F, Rudnicki MA, 2007 Asymmetric self-renewal and commitment of satellite stem cells in muscle. Cell 129 (5), 999–1010. [PubMed: 17540178]

Soukup T, Zacharova G, Smerdu V, 2002 Fibre type composition of soleus and extensor digitorum longus muscles in normal female inbred Lewis rats. Acta Histochem 104 (4), 399–405. [PubMed: 12553710]

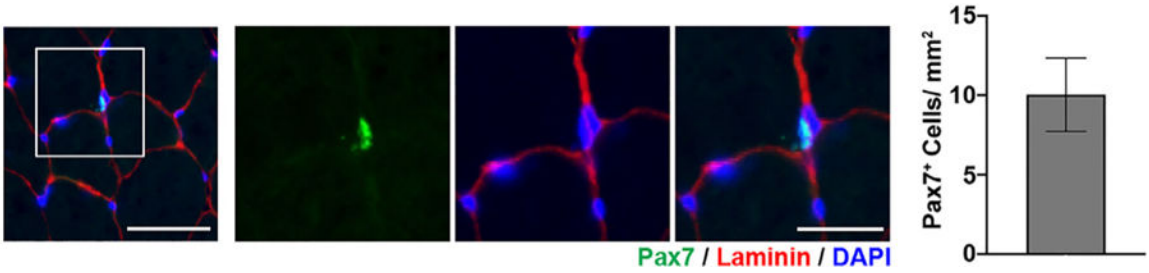

Fig. 1.

MuSCs localization. MuSCs identified by Pax7 expression in the rat Tibialis Anterior (TA) muscle. Left: low magnification image of TA (scale bar 50 μm). Center: Zoomed in images of Pax7+ cell (scale bar 25 μm). Right: quantification of Pax7+ cells.

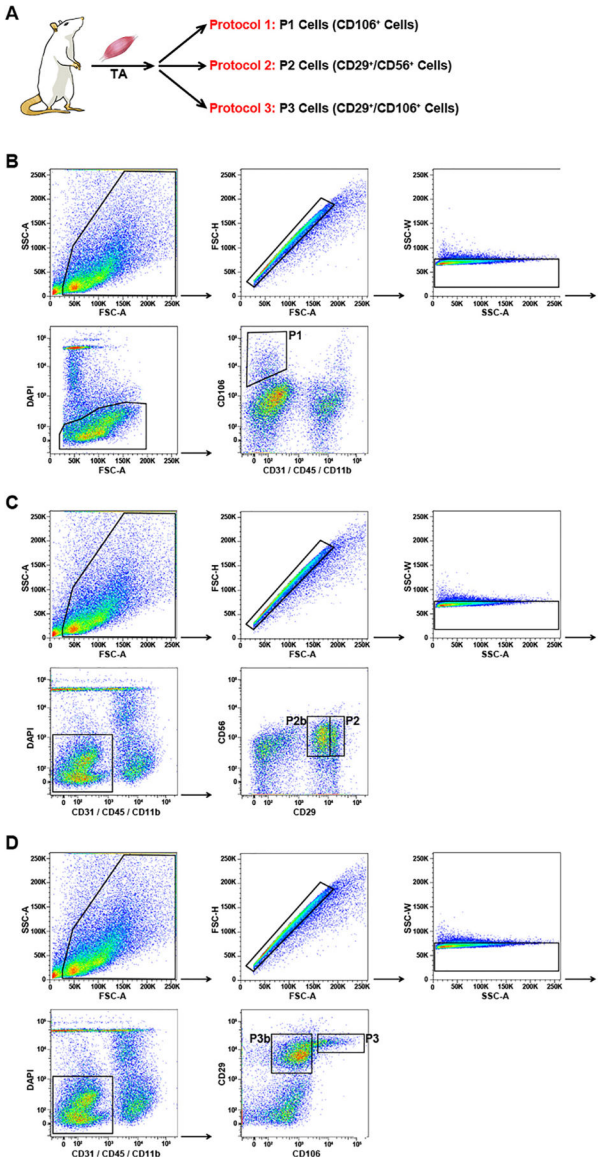

Fig. 2.

Gating approach for cell isolation protocols. (A) Experimental design for panels B–D. (TA: Tibialis Anterior). FACS plots for the gating approach used in protocols 1 (B), 2 (C), and 3 (D).

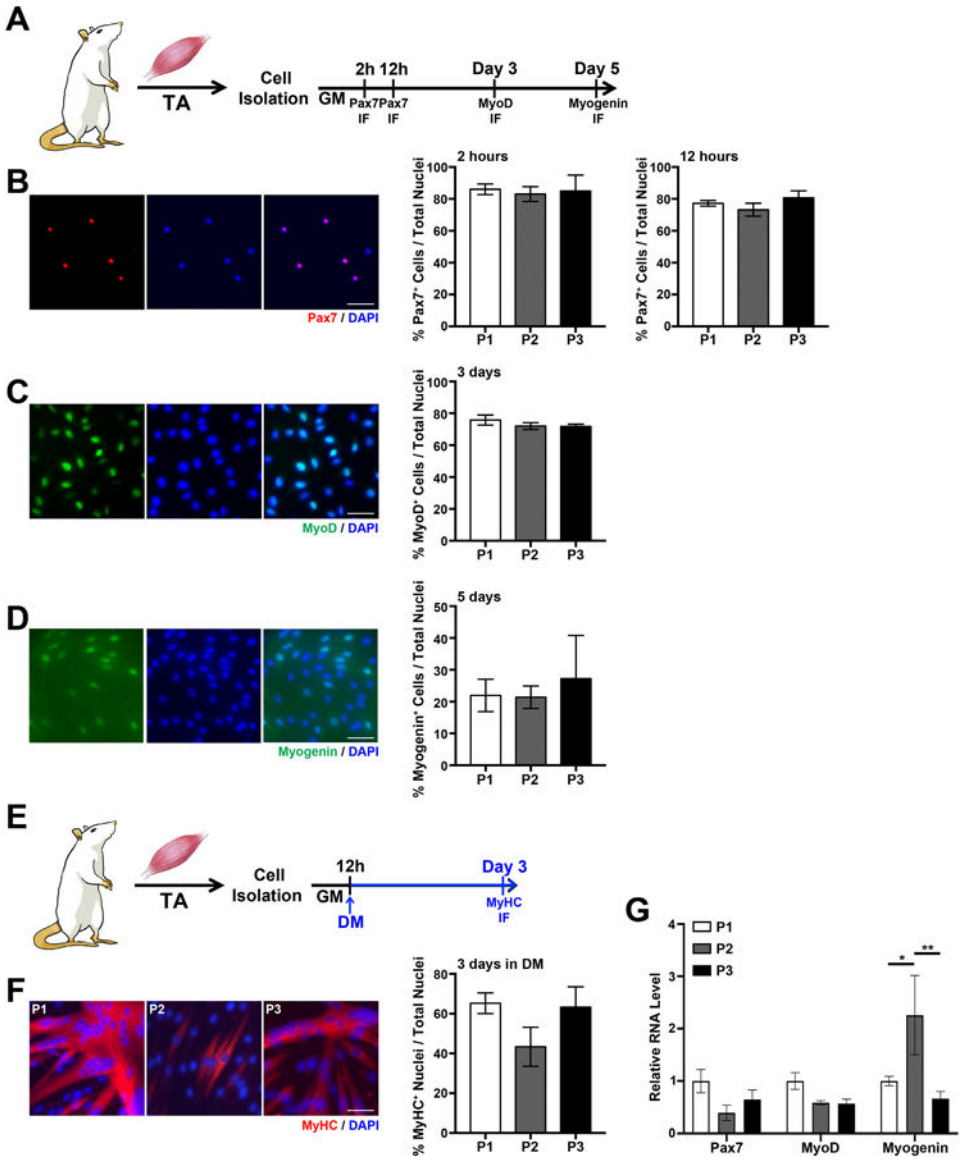

Fig. 3.

Phenotypic validation of cell populations isolated using three protocols. (A) Experimental design for panels B-D (TA: Tibialis Anterior; IF: immunofluorescence; GM: Growth Media). (B) Left: Pax7 expression in freshly isolated cells (scale bar 50 μm); right: quantification of Pax7+ cells plated for 2 and 12 h after isolation. (C) Left: MyoD expression in cultured cells (scale bar 50 μm); right: quantification of MyoD+ cells in culture for 72 h. (D) Left: myogenin expression in cultured cells (scale bar 100 μm); right: quantification of Myogenin+ cells in culture for 120 h. (E) Experimental design for panel F. (DM: Differentiation Media). (F) Left: myosin heavy chain (MyHC) expression in differentiated cells (scale bar 50 μm); right: quantification of MyHC + nuclei after 72 h in DM. (G) Quantitative real time PCR in freshly isolated cells for myogenic genes (Pax7, MyoD, Myogenin), comparing P1, P2, and P3 populations. All data are normalized to P1 population.

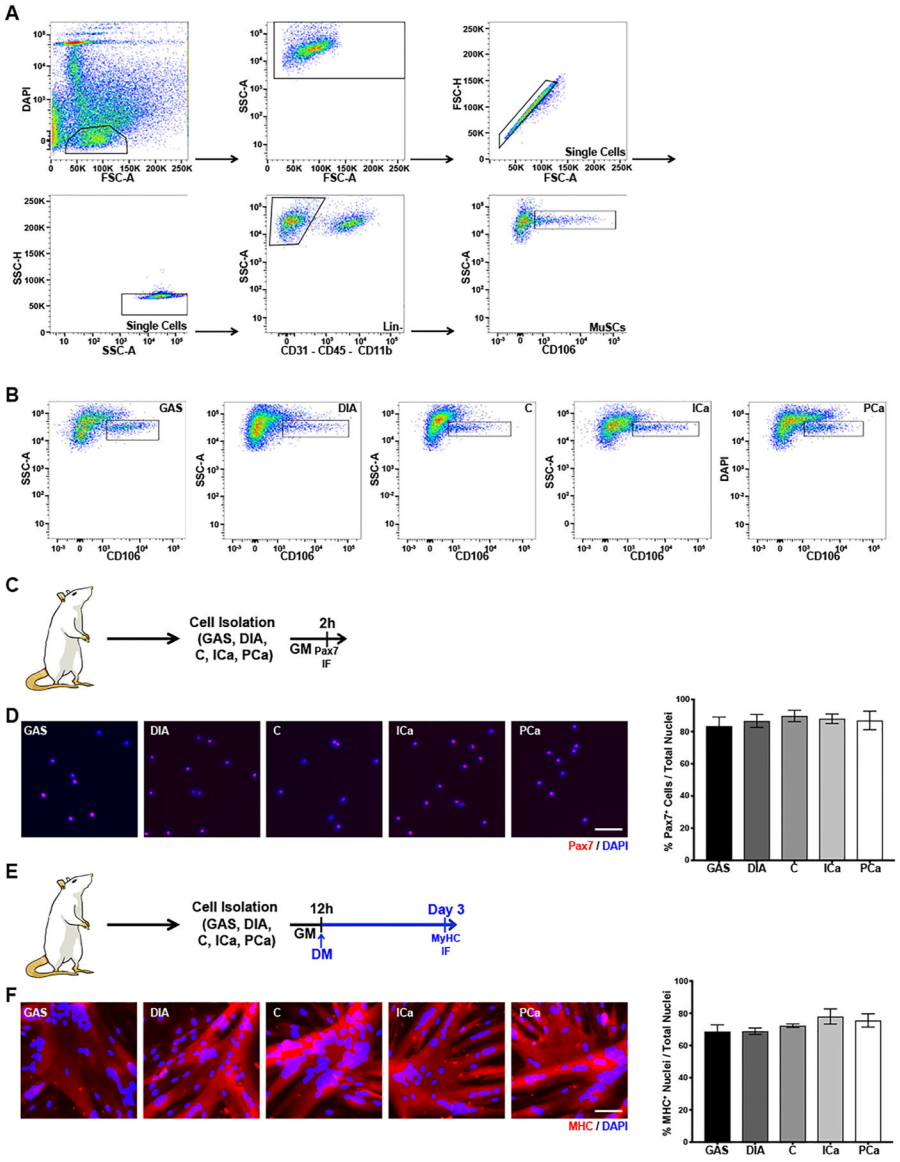

Fig. 4.

Phenotypic validation of cells isolated using Protocol 1 in gastrocnemius, diaphragm, and pelvic floor muscles. (A) FACS plots for the optimized gating for protocol 1. (GAS: Gastrocnemius; DIA: Diaphragm; C: coccygeus; ICa: iliocaudalis; PCa: pubocaudalis; GM: Growth Media; IF: immunofluorescence). (B) FACS plots showing MuSCs (black gate) in GAS, DIA, C, ICa, and PCa. (C) Experimental design for panel D. (D) Left: Pax7 expression in freshly isolated cells (scale bar 50 μm); right: quantification of Pax7+ cells plated for 2 h after isolation. (E) Experimental design for panel F. (DM: Differentiation Media). (F) Left: MyHC expression in differentiated cells (scale bar 50 μm); right: quantification of MyHC + nuclei after 72 h in DM.

KEY RESOURCES TABLE

Reagent or resource	Source	Identifier
Antibodies		
PE/Cy7 anti-mouse/rat CD29 antibody	Biolegend, USA	Cat#102221, RRID:AB_528789
Mouse NCAM-1/CD56 PE-conjugated antibody	R&D Systems, USA	Cat# FAB7820P
PE anti-rat CD106 antibody	Biolegend, USA	Cat#200403, RRID:AB_2214210
Alexa Fluor® 647 mouse anti-rat CD45	BD Biosciences, USA	Cat#565465, RRID:AB_2739250
APC mouse anti-rat CD11b	BD Biosciences, USA	Cat#562102, RRID:AB_10896148
CD31/PECAM-1 antibody (TLD) [Alexa Fluor® 647]	Novus, USA	Cat# NB100– 64796AF647
Anti-Laminin antibody produced in rabbit	Sigma-Aldrich, USA	Cat# L9393, RRID:AB_477163
Pax7	DSHB, USA	Cat# Pax7-c
Purified mouse anti-MyoD	BD Biosciences, USA	Cat#554130, RRID:AB_395255
Purified mouse anti-Myogenin	BD Biosciences, USA	Cat#556358, RRID:AB_396383
MyHC	DSHB, USA	Cat# Mf20-c
Goat anti-rabbit IgG (H+L) cross-adsorbed secondary antibody, Alexa Fluor 546	Thermo Fisher Scientific, USA	Cat# A11035, RRID:AB_2534093
Goat anti-mouse IgG1 Cross-adsorbed secondary antibody, Alexa Fluor 488	Thermo Fisher Scientific, USA	Cat# A21121, RRID:AB_2535764
DAPI solution (1mg/mL)	Thermo Fisher Scientific, USA	Cat#62248
Chemicals, Peptides, and Recombinant Proteins		
Ham's F-10 Nutrient Mix	Life Technologies, USA	Cat#11550043
Horse Serum	Sigma-Aldrich, USA	Cat#H1270–550ML
Collagenase, type II, powder	Life technologies, Gibco®, USA	Cat#17101015
Dispase II, powder	Life technologies, Gibco®, USA	Cat#17105041
Laminin	Roche®, Switzerland	Cat#11243217001
DMEM, low glucose, Pyruvate	Life technologies, Gibco®, USA	Cat#11885092
Fetal bovine serum, qualified, heat inactivated, United States	Life technologies, Gibco®, USA	Cat#16140071
Penicillin-Streptomycin (10000 U/mL)	Life technologies, USA	Cat#15140163
Pepro Tech Inc human FGF-basic (154 a.a), Recombinant protein, 100ug	Fisher Scientific, USA	Cat#50398738
PBS, Ph 7.4	Fisher Scientific, USA	Cat#10010023
Paraformaldehyde, 90%, Acros Organics™	Fisher Scientific, USA	Cat#169650025
Donor goat serum	Gemini Bio-Products, USA	Cat#100–109
Triton X-100	Sigma-Aldrich, USA	Cat# X100–500ML
Antigen unmasking solution, citric acid based	Vector Laboratories, USA	Cat# H3300, RRID:AB_2336226
Critical Commercial Assays		
miRNeasy Micro kit	Qiagen, USA	Cat#217084
QIAxpert Slide-40	Qiagen, USA	Cat#990700
SuperScript VILO cDNA Synthesis kit	Invitrogen, USA	Cat#11754050
SYBR green PCR master Mix	Life Technologies, USA	Cat#4367659
Experimental Models: Organisms/Strains		

Reagent or resource	Source	Identifier
Rat: Sprague Dawley outbred rat	Envigo, USA	RGD Cat# 737903, RRID:RGD_737903
Software and Algorithms		
Adobe Photoshop CS4	Adobe, USA	NA
ImageJ	ImageJ, USA	NA
Prism 7 and Prism 8	GraphPad Software, Inc., USA	NA